BIOCHEMISTRY
including biophysical chemistry & molecular biology
Article

Sulfide Binding Properties of Truncated Hemoglobins[†]

Francesco P. Nicoletti,[§] Alessandra Comandini,[‡] Alessandra Bonamore,[‡] Leonardo Boechi,[||] Fernando Martin Boubeta,[||] Alessandro Feis,[§] Giulietta Smulevich,[§] and Alberto Boffi*[,‡]

[‡]*Istituto Pasteur, Fondazione Cenci-Bolognetti, Department of Biochemical Sciences and CNR Institute of Molecular Biology and Pathology, University of Rome "La Sapienza," Piazzale Aldo Moro 5, I-00185 Rome, Italy,* [§]*Dipartimento di Chimica, Università di Firenze, Via della Lastruccia 3, I-50019 Sesto Fiorentino (FI), Italy, and* [||]*Departamento de Química Inorgánica, Analítica, y Química Fisica, INQUIMAE-CONICET, Facultad de Ciencias Exactas y Naturales, Universidad de Buenos Aires, Ciudad Universitaria, Buenos Aires, Argentina*

ABSTRACT: The truncated hemoglobins from *Bacillus subtilis* (Bs-trHb) and *Thermobifida fusca* (Tf-trHb) have been shown to form high-affinity complexes with hydrogen sulfide in their ferric state. The recombinant proteins, as extracted from *Escherichia coli* cells after overexpression, are indeed partially saturated with sulfide, and even highly purified samples still contain a small but significant amount of iron-bound sulfide. Thus, a complete thermodynamic and kinetic study has been undertaken by means of equilibrium and kinetic displacement experiments to assess the relevant sulfide binding parameters. The body of experimental data indicates that both proteins possess a high affinity for hydrogen sulfide ($K = 5.0 \times 10^6$ and 2.8×10^6 M^{-1} for Bs-trHb and Tf-trHb, respectively, at pH 7.0), though lower with respect to that reported previously for the sulfide avid *Lucina pectinata* I hemoglobins (2.9×10^8 M^{-1}). From the kinetic point of view, the overall high affinity resides in the slow rate of sulfide release, attributed to hydrogen bonding stabilization of the bound ligand by distal residue WG8. A set of point mutants in which these residues have been replaced with Phe indicates that the WG8 residue represents the major kinetic barrier to the escape of the bound sulfide species. Accordingly, classical molecular dynamics simulations of SH^--bound ferric Tf-trHb show that WG8 plays a key role in the stabilization of coordinated SH^- whereas the YCD1 and YB10 contributions are negligible. Interestingly, the triple Tf-trHb mutant bearing only Phe residues in the relevant B10, G8, and CD1 positions is endowed with a higher overall affinity for sulfide characterized by a very fast second-order rate constant and 2 order of magnitude faster kinetics of sulfide release with respect to the wild-type protein. Resonance Raman spectroscopy data indicate that the sulfide adducts are typical of a ferric iron low-spin derivative. In analogy with other low-spin ferric sulfide adducts, the strong band at 375 cm^{-1} is tentatively assigned to a Fe–S stretching band. The high affinity for hydrogen sulfide is thought to have a possible physiological significance as H_2S is produced in bacteria at metabolic steps involved in cysteine biosynthesis and hence in thiol redox homeostasis.

Truncated hemoglobins (trHbs) make up a family of globins that are widely distributed among bacteria, protozoa, and plants (*1, 2*). These proteins are characterized by a remarkable variability in the nature of the heme pocket residues among the various species (*1*), thus suggesting diverse functions, possibly related to the physiological response in the defense from oxygen reactive species and/or NO (*2*). The variability of the amino acid residues of the distal heme pocket suggested the partition of trHbs in three groups that share less than 30% sequence similarity with each other (*1*). In the three groups, the proximal F8 histidine is invariant and the B9 and B10 pair is commonly phenylalanine and tyrosine, respectively, whereas other residues lining the heme pocket are not conserved. Group II is by far the most populated among the three and is characterized by the presence of a Trp residue on the bottom of the heme distal pocket (G8 position, according to the classical globin nomenclature).

The crystal structures of group II truncated hemoglobins thus obtained from *Bacillus subtilis* (Bs-trHb)[1] (*3*), *Thermobifida fusca* (Tf-trHb) (*4*), *Geobacillus stearothermophilus* (Gs-trHb) (*5*), and *Mycobacterium tuberculosis* (Mt-trHbO) (*6, 7*) revealed a common general pattern for the heme pocket that is characterized by an ensemble of polar residues in contact with the iron-bound ligand coordination shell (*8, 9*). The biological significance of such an unusual network of interactions is unexplained, although the thermodynamic consequence is thought to account for the high oxygen affinity displayed by the group II trHbs hitherto investigated (*3–6, 9*).

However, since the beginning of our investigations of group II truncated hemoglobins, several UV–visible and/or resonance Raman observations were biased by the presence of supposed artifacts of the respective spectra. In particular, even in highly purified samples, the presence of small but significant amounts of

[1]Abbreviations: Bs-trHb, truncated hemoglobin from *B. subtilis*; Tf-trHb, truncated hemoglobin from *T. fusca*; 3F-Tf-trHb, YB10F/YCD1F/WG8F triple mutant; Gs-trHb, truncated hemoglobin from *G. stearothermophilus*; PMB, *p*-chloromercuric benzoate; RR, resonance Raman; 6cLS, six-coordinate low-spin.

low-spin adducts often hampered a clean interpretation of experimental results. At least in one case (*10*), the low-spin ferric adduct, present within dithionite-containing solutions, was attributed to the formation of a stable ferric derivative with some dithionite byproduct, possibly sulfide. The presence of a ferric sulfide adduct with a typical visible absorption spectrum peak at 426 nm was then reproducibly observed in Bs-trHb and Tf-trHb preparations immediately after cell disruption, thus indicating that these proteins were at least partially saturated with sulfide within the *Escherichia coli* expression vector and were endowed with a high affinity for this ligand.

To date, the first and unique experimental evidence of high-affinity sulfide binding hemoglobin is represented by hemoglobin I (HbI) from the mollusk *Lucina pectinata*, a monomeric protein that binds sulfide (H$_2$S) in its ferric state. This hemoglobin is one of the few known H$_2$S carriers in living organisms that have been implicated in physiologically binding and transporting this toxic gas in the ferric heme iron center (*11*). The affinity of hydrogen sulfide for ferric HbI is exceptionally high compared to those for other hemoglobins and is achieved through fast association and very slow dissociation processes (*11*, *12*). The ability of HbI to bind H$_2$S with such high affinity has been considered unique for this hemoglobin. However, given the potential sulfide binding properties of hemoglobins and the active sulfur metabolism of microorganisms, biochemical functions other than transport of the gaseous ligand might be hypothesized. In this framework, it is useful to outline the key metabolic steps of sulfide metabolism in microorganisms. Many bacteria reduce inorganic sulfate to sulfide for the purpose of incorporation into newly synthesized molecules through the so-called pathways of assimilatory sulfate reduction. In many bacteria and lower eukaryotes, assimilatory sulfate reduction proceeds via activation of sulfate to APS (adenosylphosphosulfate) by the enzyme sulfate adenylyltransferase. Following sulfate activation, a final reduction of sulfite to sulfide is catalyzed by a sulfite reductase enzyme (encoded by the cysJ and cysI genes in *E. coli*) (*13*). This enzyme, catalyzing the six-electron reduction of sulfite to sulfide, is a complex hemoflavoprotein and is the major source of free H$_2$S in microorganisms. In the bacterium *E. coli*, H$_2$S thus produced is a substrate of cysteine synthase isozymes, which are under the positive control of the cysteine-responsive CysB transcriptional dual regulator (that governs the expression of the whole cysteine operon). *E. coli* K-12 produces two cysteine synthase isoenzymes (cysteine synthase A and cysteine synthase B). Cysteine synthase B is preferentially used for the biosynthesis of L-cysteine during anaerobic growth conditions (*14*) and is able to utilize thiosulfate instead of sulfide to produce *S*-sulfo-L-cysteine (*15*). The pathway step is reversible, and genetic and proteomic data suggest that the cysteine synthases may actually act as a sulfur scavenging system during sulfur starvation, stripping sulfur off of L-cysteine. In this context, the presence of a sulfide avid globin (either constitutively expressed or recombinant) might compete with the sulfide scavenging activity of cysteine synthases, stimulate the activation of the CysB regulator, or alter the homeostasis of the overall thiol redox status.

The question of whether this finding for truncated hemoglobin might have biochemical and/or physiological relevance prompted this investigation, based on the spectroscopic, molecular dynamics, thermodynamic, and kinetic characterization of Bs-trHb and Tf-trHb in their reaction with sulfide. The objective is to pave the way to dedicated researches addressing the potentially complex interplay between globins and metabolic pathways involving physiologically relevant sulfur compounds.

EXPERIMENTAL PROCEDURES

Expression Cloning. The truncated hemoglobins from *B. subtilis* and *T. fusca* were expressed as recombinant proteins in *E. coli* cells and purified as described previously (*3*, *4*). Point mutants YB10F, YCD1F, and WG8F and the triple mutant of *T. fusca* (3F-Tf-trHb) were obtained by PCR using standard procedures. The PCR products were cloned into the pET28b expression vector (Invitrogen Co.) following the manufacturer's instructions, and the recombinant plasmids were transformed into *E. coli* TOP 10 cells. Plasmid DNA was purified and transformed into *E. coli* TUNER(DE3) cells (Novagen, Merck KGaA) for expression. The integrity of the cloned gene was verified by DNA sequencing. Strains bearing recombinant expression vectors were grown under different conditions, namely in shake flasks or in Sartorius 2 L fermentors with feed batch procedures to optimize protein expression (see Results). Growth experiments were conducted at 25 and 30 °C via comparison of LB broth to M9 minimal broth and via adjustment of oxygen supply from 20% constant flow (in fermentor) to aerated shake flasks to sealed shake flasks. The best expression conditions (at the expense of the total biomass) were in LB broth in sealed shake flasks, at 25 °C. Single and triple mutants were extracted and purified according to the same procedure used for the wild-type (wt) protein.

Spectroscopic Characterization. (*i*) *Electronic Absorption*. UV−visible absorption spectra were recorded on a Jasco V-570 spectrophotometer (Jasco Ltd.) and with a double-beam Cary 5 spectrophotometer (Varian, Palo Alto, CA). The protein concentration was determined on the CO derivative in the presence of 10−20 mM sodium dithionite by using an extinction coefficient of 178000 M^{-1} cm^{-1} at 421 nm for Bs-trHb and 174000 M^{-1} cm^{-1} for Tf-trHb. In all measurements, the dithionite concentration was constantly kept below 20 mM and CO gas was added before or immediately after dithionite addition to prevent the formation of the sulfide adduct.

(*ii*) *Resonance Raman Scattering*. The sulfide complexes were prepared by addition of sodium sulfide to the protein solution in 100 mM phosphate buffer (pH 7.0). Protein concentrations were in the range of 15−30 μM. An excess of sulfide was needed in RR experiments to compensate for the progressive release of H$_2$S and the sulfide oxidation that unavoidably occurs during the relatively long time needed for the measurements at 25 °C and in aerated Raman cells.

RR spectra were recorded with the 413.1 nm line of a Kr$^+$ laser (Coherent, Innova 300 C) and 1.2 cm^{-1} spectral resolution The back-scattered light from a slowly rotating NMR tube was collected and focused into a triple spectrometer (consisting of two Acton Research SpectraPro 2300i instruments working in subtractive mode and a SpectraPro 2500i instrument in the final stage with a grating of 3600 grooves/mm), equipped with a liquid nitrogen-cooled CCD detector (Roper Scientific, Princeton Instruments). The RR spectra were calibrated with indene, CCl$_4$, and pyridine as standards to an accuracy of 1 cm^{-1} for intense isolated bands.

Sulfide Determination. The sulfide concentration was measured by using the *p*-chloromercuribenzoate (PMB, Sigma Aldrich) method according to Boyer (*16*). Standard sulfide solutions were obtained by dissolving vacuum-dried sodium

sulfide nonahydrate [Na$_2$S(H$_2$O)$_9$, Sigma Aldrich Co.] in the desired buffer in stoppered vials under nitrogen and used within 24 h. Determination of the amounts of iron-bound sulfide in Bs-trHb and Tf-trHb proteins was accomplished by the PMB method by following the absorbance increase at 250 nm (formation of the PMB sulfide adduct) and concomitant absorbance decrease at 425 nm (release of sulfide from the heme iron) in an HP 8453 diode array spectrophotometer. Typically, a solution containing 35 μM protein in 20 mM Hepes buffer (pH 7.0) was mixed with a 1.2-fold molar excess of PMB in a double-sector quartz cell (0.45 cm × 2 cm, optical path length), and spectra were recorded at 10 min intervals over 2 h at 25 °C.

Azide−Sulfide Displacement Experiments. Sulfide binding thermodynamics were assessed in ligand displacement experiments by using sodium azide and sodium sulfide as competing ligands in 0.1 M phosphate buffer (pH 7.0) at 25 °C. Experiments were conducted via titration of 10 μM protein solutions saturated with 1, 10, or 100 mM azide, with a buffered sodium sulfide solution (0.1 M). Spectra were recorded on an HP 8453 diode array spectrophotometer, and binding curves were generated by standard procedures. The apparent equilibrium constants were thus obtained with the equation $K_{app} = K_{(HS^-)}/[K_{(N_3^-)}[N_3^-]]$.

Sulfide and azide second-order binding kinetics were recorded with an Applied Photophysics stopped flow apparatus (Applied Photophysics, Leatherhead, U.K.) by mixing protein solutions (10 μM) with sulfide or azide solutions in 0.1 M phosphate (pH 7.0) at 25 °C. Second-order rate constants were calculated by least-squares fitting methods using standard procedures. Sulfide and azide release kinetics were measured independently by two different procedures. Sulfide release kinetics was first measured by mixing a sulfide-saturated protein solution (10 μM protein in the presence of 10 μM sulfide) with a 2-fold molar excess of PMB [or ZnCl$_2$ or Pb(CH$_3$COOH)$_2$] or alternatively with a 100 mM azide solution. Time courses were monitored on a spectrophotometer at 425 nm over 3 h and were essentially superimposable with the different metals or azide. Azide release kinetics were measured in the stopped flow apparatus by mixing an azide-saturated protein solution (10 μM protein in the presence of 10 mM azide) with 10−1000 μM sulfide solutions. Time courses, measured at 425 or 414 nm, were independent of sulfide concentration and thus entirely attributed to the release of the azide ion.

Molecular Dynamics Simulations. The simulations were performed starting from the crystal structure of wild-type Tf-trHb, determined at 2.48 Å resolution [Protein Data Bank (PDB) entry 2BMM] (3). The SH$^-$ was added in the distal side according to the equilibrium structure in QM calculus, taking into account the distal site environment. The system was then immersed in a box of TIP3P water molecules (17). The minimum distance between the protein and wall was 12 Å. All systems were simulated employing periodic boundary conditions and Ewald sums for treating long-range electrostatic interactions (18). The shake algorithm was used to keep bonds involving the H atom at their equilibrium length. This allowed us to employ a 2 fs time step for the integration of Newton's equations. The parm99 and TIP3P force fields implemented in AMBER were used to describe the protein and water, respectively (19). The heme with coordinated sulfide model system charges was assessed as described in previous works (20). The temperature and pressure were regulated with the Berendsen thermostat and barostat, respectively, as implemented in AMBER.

All systems were minimized to optimize any possible structural clashes. Subsequently, the systems were heated slowly from 0 to
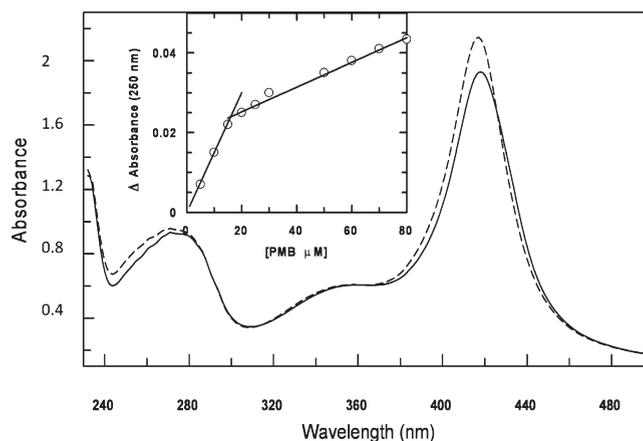

FIGURE 1: Iron-bound sulfide determination in Bs-trHb. A Bs-trHb hemoglobin solution (33 μM) and a PMB solution (35 μM) were placed in a double sector quartz cell (0.45 cm each sector) (—). After the solutions had been mixed (---), the increase in absorbance at 250 nm (formation of the PMB sulfide adduct) is paralleled by a spectral shift of the Soret band (release of sulfide from the heme iron) toward shorter wavelengths. The inset shows a PMB titration experiment that included addition of small aliquots of a PMB solution to a 150 μM Bs-trHb solution. The increase in absorbance at 250 nm is plotted vs PMB concentration. Experiments were conducted in 20 mM Hepes buffer (pH 7.0) at 20 °C.

300 K using a time step of 0.1 fs, under constant volume conditions. Finally, a short simulation at a constant temperature of 300 K under a constant pressure of 1 bar was performed using a time step of 0.1 fs, to allow the systems to reach proper density. These equilibrated structures were the starting point for 15 ns of MD simulations.

Mutations were performed in silico by changing the corresponding amino acid in the original structure and allowing the system to equilibrate as mentioned above.

RESULTS

Sulfide Determination. The presence of iron-bound sulfide in Bs-trHb and Tf-trHb was initially determined on highly purified proteins (a single band on SDS gel electrophoresis) with PMB as a chromophoric sulfide scavenger. All samples tested (four independent preparations), conducted with horse heart myoglobin as a control, showed the presence of 6−15% sulfide in Bs-trHb, 3−7% sulfide in Tf-trHb, and none in horse heart myoglobin, with an error of 1.6% (Figure 1). In all experiments, the increase in the magnitude of the PMB signal at 250 nm (mercuric sulfide adduct formation) was paralleled by a shift of the relevant Soret band at shorter wavelengths (from ∼420 to 416 nm), thus confirming that release of sulfide from the protein occurred. A similar experiment was conducted with the same proteins during an earlier stage of the purification by using ZnCl$_2$ or Pb(CH$_3$COOH)$_2$ in 10-fold molar excess as a sulfide scavenger (in 10 mM Hepes buffer). No PMB can be used in this case because of the presence of possible free thiol groups of contaminating proteins. The same spectral shift of the Soret band was observed, though to a larger extent with respect to the shift observed in the purified protein. These results demonstrate that both Bs-trHb and Tf-trHb are partially bound with sulfide within the cell (*E. coli*) and must possess a high affinity for the anion such that a small but significant amount of sulfide is still bound to the heme iron after the complete purification procedure. A screening of the cell growth conditions was also conducted to increase the level of recombinant protein expression and, in parallel, to discriminate possible environmental contribution to
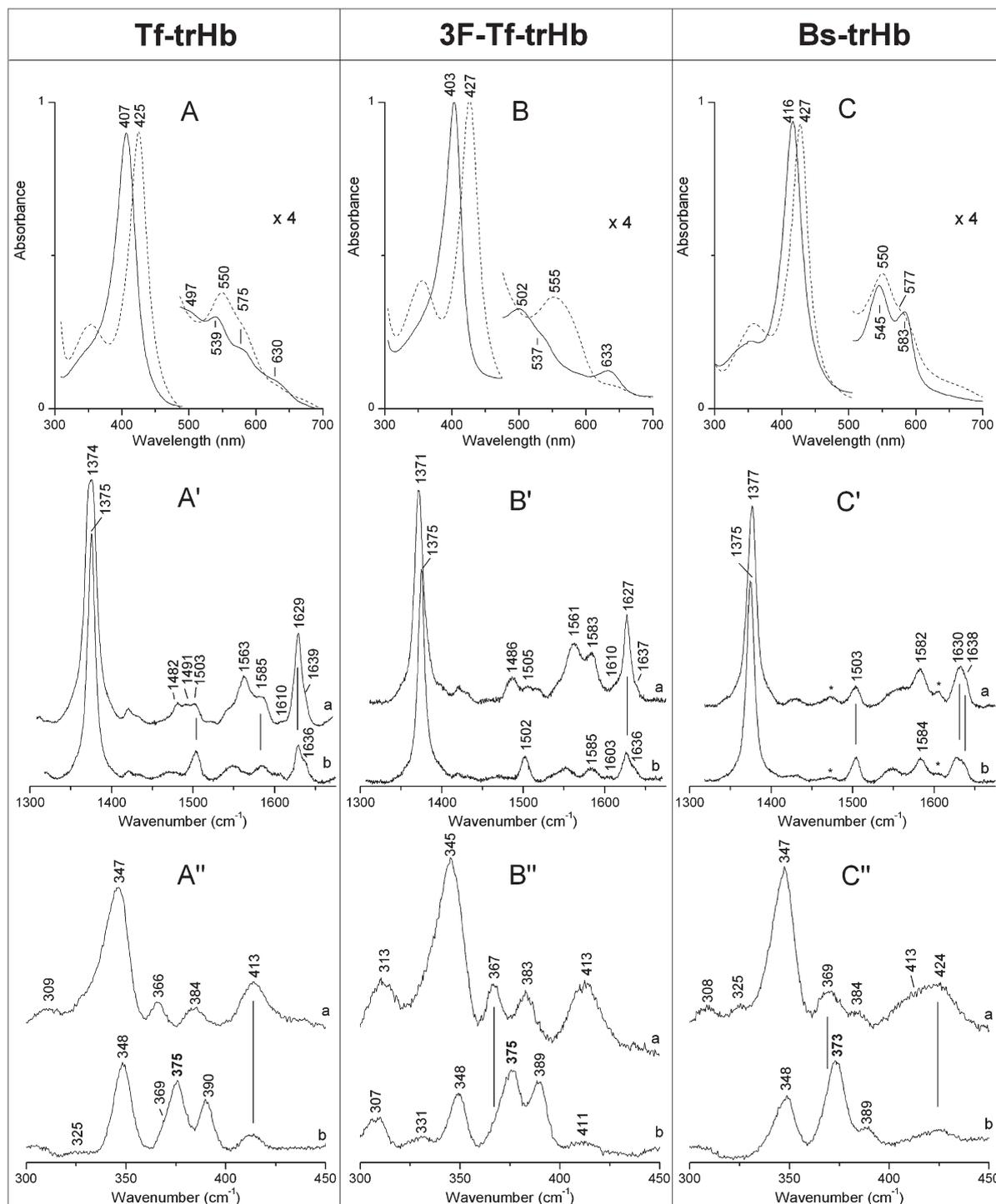
FIGURE 2: Visible absorption and resonance Raman spectra of ferric *T. fusca*, its triple mutant, *B. subtilis*, and their sulfide adducts. (A−C) Absorption spectra of Tf-trHb (A), 3F-Tf-trHb (B), and Bs-trHb (C) at pH 7 in 100 mM phosphate buffer (—) and in the presence of a 5 mM Na$_2$S solution (---). (A′−C′) High-frequency RR spectra of Tf-trHb (A′), 3F-Tf-trHb (B′), and Bs-trHb (C′): 2 mW laser power at the sample and an average of three spectra with an integration time of 720 s (a) or in the presence of a 5 mM Na$_2$S solution with a 10 mW laser power at the sample and an average of three spectra with an integration time of 540 s (b). The asterisk indicates spurious bands of the deoxy form deriving from the photolysis of the ferrous−oxy species present in Bs-trHb in small quantities (3). (A″−C″) Low-frequency RR spectra of Tf-trHb (A″), 3F-Tf-trHb (B″), and Bs-trHb (C″). The protein concentrations were 30 μM: 2 mW laser power at the sample and an average of six spectra with an integration time of 1800 s (a) or in the presence of a 5 mM Na$_2$S solution with a 10 mW laser power at the sample and an average of two spectra with an integration time of 1800 s (b). The $\nu_{(Fe-S)}$ is indicated in bold.

the generation of hemoglobin sulfide adducts. Interestingly, the best protein expression and minimal sulfide saturation were observed under minimal oxygen concentrations at 25 °C (in sealed shake flasks). In contrast, growth with a high level of oxygen in fermentors (20% with a constant air supply) resulted in a 10-fold decreased level of protein expression and a much higher

level of sulfide saturation. Because of the higher protein:biomass ratio, all experiments were conducted with proteins extracted from cells grown in sealed shake flasks at 25 °C.

Spectroscopic Characterization. UV−visible absorption spectra of the sulfide adducts of Tf-trHb, triple mutant YB10F/YCD1F/WG8F (3F-Tf-trHb), and Bs-trHb are reported

Table 1: Iron−Sulfur Stretching Frequencies in Heme Proteins

protein	mode	frequency (cm^{-1})	ref
cytochrome P$_{450cam}$	Fe^{3+}−S$_{Cys}$	351 (-5 cm^{-1} in ^{34}S; 2.5 cm^{-1} in ^{54}Fe)	35
chloroperoxidase	Fe^{3+}−S$_{Cys}$	347 (-5 cm^{-1} in ^{34}S)	36
nitric oxide reductase	Fe^{3+}−S$_{Cys}$	342	37
nitric oxide reductase	Fe^{3+}−S$_{Cys}$	338 (-1 cm^{-1} in ^{57}Fe; 2 cm^{-1} in ^{54}Fe)	38
superoxide reductase	Fe^{3+}−S$_{Cys}$	298−328 region (many bands with Fe−S contribution)	39
cytochrome *c*	Fe^{2+}−S$_{Met80}$	372 in ^{57}Fe^{2+} (377 in ^{54}Fe^{2+}) (375 in ^{57}Fe^{3+})	40
L. pectinata HbI	Fe^{3+}−S	374	21
B. subtilis trHb	Fe^{3+}−S	375	this work
T. fusca trHb	Fe^{3+}−S	375	this work
T. fusca 3F mutant	Fe^{3+}−S	373	this work
T. fusca WG8F mutant	Fe^{3+}−S	375	this work
T. fusca YCD1F mutant	Fe^{3+}−S	374	this work

in Figure 2 (panels A−C, respectively) in comparison with those of the native ferric derivatives. Spectra of two single point mutants of Tf-trHb (YCD1F and WG8F) are reported as Supporting Information (Figure S3). All spectra of the sulfide-bound forms display an absorption profile that is characteristic of the low-spin sulfide adduct as reported for *L. pectinata* HbI, with a Soret band centered at 425−427 nm and a broad visible band at 550−575 nm (*11, 12*). Accordingly, the resonance Raman spectra (Figure 2A′−C′) of the sulfide complexes displayed typical ferric, low-spin iron features with ν_3 at 1502−1503 cm^{-1}, ν_2 at 1584−1585 cm^{-1}, and ν_{10} at 1636−1638 cm^{-1}, as previously reported for *L. pectinata* HbI (*21*). Moreover, in the low-frequency region (Figure 2A″−C″), a strong band at 373−375 cm^{-1} that appears upon sulfide complexation is tentatively assigned to the ν(Fe−S) stretching mode in analogy to HbI (Table 1). In the ferric samples, the two bands at 366−369 and 383−384 cm^{-1} are tentatively assigned to heme propionyl bending vibrations [$\delta(C_\beta C_c C_d)$] (*22*). The different frequencies of the two propionyl bending modes suggest that while one propionyl has a weaker H-bonding interaction (366−369 cm^{-1}), the other experiences a stronger H-bonding network (383−384 cm^{-1}). In fact, the frequencies of these modes have been proposed to shift to higher frequencies as a result of hydrogen bonding between the propionyl groups of the heme and nearby amino acid side chains, although there is not a fixed relationship between a given frequency and the number of hydrogen bonds (*23, 24*). Inspection of the crystal structures of Tf-trHb and Bs-trHb (*3, 4*) provides a rationale for the observed frequencies. In particular, while the 7-propionyl group interacts with a water molecule at 2.7 Å (for Tf-trHb) and Thr45 at 2.9 Å (for Bs-trHb), the 6-propionyl group is involved in a wider hydrogen bonding network (for Tf-trHb, Arg105, Arg97, and Tyr93 at 3.2, 2.9, and 2.7 Å, respectively; for Bs-trHb, Lys48 and Tyr63 at 2.2 and 2.4 Å, respectively). Thus, the modes at 384 cm^{-1} can be assigned to the bending vibrations of the heme substituent at position 6. It is worth noting that when sulfide binds the band at 383−384 cm^{-1} (Figure 2A″−C″) upshifts by 5−6 cm^{-1} whereas the band at 369 cm^{-1} does not appear to be affected.

RR spectra of the sulfide adducts of two single point mutants of Tf-trHb (YCD1F and WG8F) are reported as Supporting Information (Figure S3) in comparison with those of the native ferric derivatives. The sulfide adduct spectra are almost identical to those of wt and 3F-Tf-trHb proteins.

Thermodynamics and Kinetics of Sulfide Binding. A complete set of azide−sulfide displacement experiments was conducted as described in Experimental Procedures with
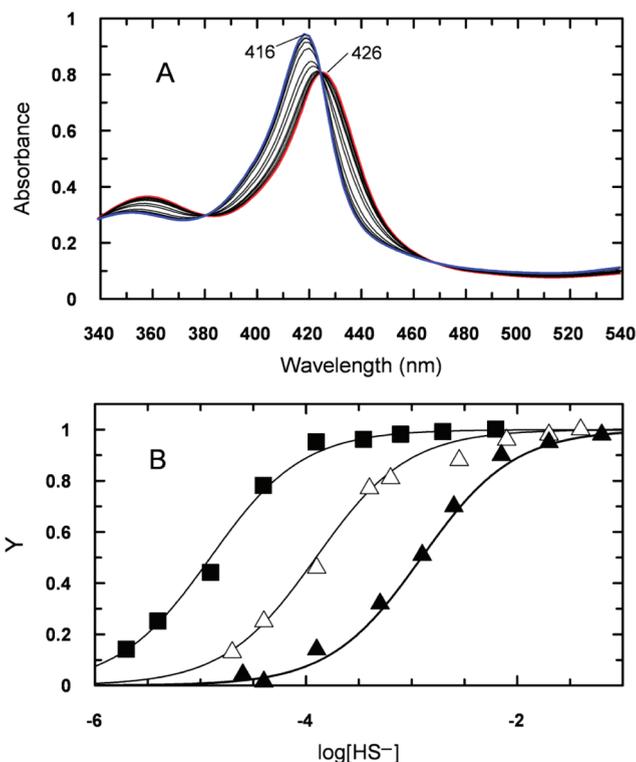

FIGURE 3: Azide−/sulfide displacement experiments in ferric Bs-trHb. A Bs-trHb solution (7 μM) saturated with 10 mM sodium azide was titrated via addition of small aliquots of a concentrated (0.1 M) sodium sulfide nonahydrate solution (A) in 0.1 M phosphate buffer (pH 7.0). Spectral line shapes peaked at 415 nm for the azide adduct shifted at 426 nm for the sulfide derivative. (B) Normalized absorbance changes at different azide concentrations (1, 10, and 100 mM sodium azide) were then plotted vs sulfide concentration. Solid lines represent the best fitting curves according to eq 1. Results are reported in Table 1 (see also the Supporting Information).

Bs-trHb and Tf-trHb and its single (YB10F, YCD1F, and WG8F) and triple (3F-Tf-trHb) mutants. Experiments, fitted to a simple ligand binding curve, yielded accurate estimates of the affinity costant (K_{app}) for the three proteins (Figure 3 and Supporting Information). To isolate the relevant second-order binding constants for sulfide [$k_{(HS^-)}$] and azide [$k_{(N_3^-)}$], a set of rapid mixing experiments was conducted (Figure S6 of the Supporting Information). Finally, sulfide and azide first-order dissociation constants were also measured according to the procedures outlined in Experimental Procedures (Figure S7 of the Supporting Information). The body of thermodynamics and kinetic data yielded the complete picture reported in Table 2.

Table 2: Thermodynamics and Kinetic Constants for Sulfide and Azide Binding to the Truncated Hemoglobins from *B. subtilis* and *T. fusca* and Its Triple Mutant[a]

protein	$K_{(N_3^-)}$ (M^{-1})	$k_{(N_3^-)}$ (M^{-1} s^{-1})	$k'_{(N_3^-)}$ (s^{-1})	$K_{(HS^-)}$ (M^{-1})	$k_{(HS^-)}$ (M^{-1} s^{-1})	$k'_{(HS^-)}$ (s^{-1})
Bs-trHb	6.2×10^4	2.9×10^5	4.6	5.0×10^6	1.3×10^4	0.0026
Tf-trHb	3.1×10^4	3.4×10^3	0.11	2.8×10^6	5×10^3	0.0018
Tf-YCD1F	1.9×10^4	6.8×10^3	0.35	5.8×10^6	5.8×10^3	0.001
Tf-YB10F	4.6×10^4	8.4×10^4	1.8	3.1×10^7	7.8×10^3	0.0012
Tf-WG8F	5.6×10^4	3.9×10^4	0.69	1.13×10^5	4.1×10^4	0.36
3F-Tf-trHb	4.4×10^5	5.5×10^4	0.125	2.0×10^7	4.4×10^6	0.22
sw Mb[b]				5×10^4	–	–
FQF sw Mb[b]				3.7×10^7	–	–
L. pectinata HbI[c]				1.1×10^7	2.3×10^5	0.00022
L. pectinata HbII[c]				1.7×10^4	1.13×10^4	0.017
L. pectinata HbIII[c]				2.5×10^4	$1–4 \times 10^4$	0.016

[a]Data obtained in 0.1 M phosphate buffer (pH 7.0) at 25 °C. Further experimental details and errors are reported in the Supporting Information. [b]Data for sperm whale myoglobin and its L29F/H64Q/V68F triple mutant (*17*). [c]Data at pH 7.5 (*K* and *k'*) or at the acid limit (*k*) (*11*).
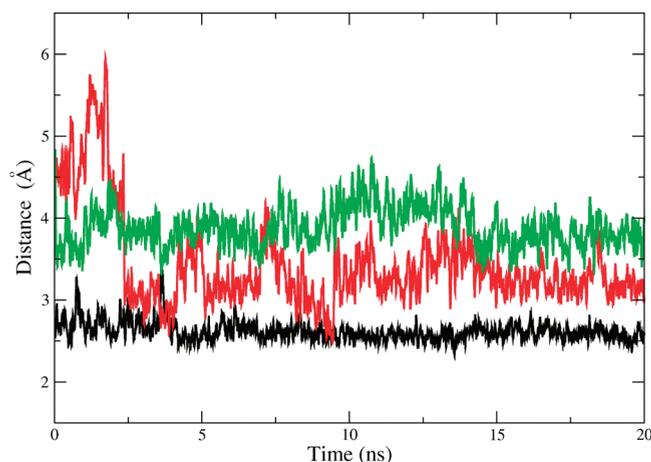

FIGURE 4: Time evolution of selected distances among distal residues and heme-bound SH$^-$ of wt Tf-trHb. The distances are defined as the distances between the S atom of the coordinated SH$^-$ and the indole N proton of WG8 (black), the hydroxyl hydrogen of YCD1 (red), and the hydroxyl hydrogen of YB10.

Molecular Dynamics Simulations. Classical molecular dynamics simulations of SH$^-$-bound ferric Tf-trHb were performed to shed light on the role of the hydrogen bond network stabilizing coordinated sulfide, and its connection with kinetic properties.

During the time scale of the simulation, we found that WG8 plays a key role in the stabilization of coordinated SH$^-$. YCD1 and YB10 are not involved in the stabilization of the ligand, which can be seen via inspection of the time evolution of the distances from the OH groups of YCD1 and YB10 to the sulfur (Figure 4). A representative snapshot is given in Figure 5. In addition, the 6-propionyl was observed to interact with Arg97, Tyr93, and Arg78 (and not Arg105, as shown in the crystal structure), and with one or two water molecules. On the other hand, the 7-propionyl is stabilized by several water molecules and by a weak interaction with Arg78 (Figure 6).

These results are in agreement with the kinetic results, in which the WG8F single mutant is the only mutant protein that affects significantly the dissociation kinetic constant (see Table 2).

DISCUSSION

These data highlight unexpected sulfide binding properties of Bs-trHb and Tf-trHb and demonstrate that these proteins are

able to bind sulfide with an affinity constant in the submicromolar range (see Table 2). Sulfide may coordinate to the heme iron in the monoprotonated form, HS$^-$, or in the diprotonated one, H$_2$S, since the p*K* for this equilibrium is reportedly ≈7. The affinity of these trHbs for sulfide is ~100-fold higher than that reported for horse (6×10^4 M^{-1}) or sperm whale (5×10^4 M^{-1}) myoglobins (*25*). Still, the sulfide affinity is ~50−100-fold lower than that reported for the sulfide avid *L. pectinata* HbI hemoglobin (2.9×10^8 M^{-1}) (*11*). A comparison between the sulfide binding properties of *L. pectinata* hemoglobins and those of the truncated hemoglobins Bs-trHb and Tf-trHb reveals several analogies but also striking differences. In all proteins, the kinetic counterpart of the thermodynamic stability of the ferric sulfide adduct is the relatively fast second-order combination kinetics and the very slow sulfide dissociation rate. All proteins are also capable of reacting with sulfide in their ferrous oxygenated forms, a reaction that is most likely accompanied by iron oxidation and release of a superoxide anion (*11*). However, *L. pectinata* HbI has been shown to promptly release sulfide upon heme iron reduction (*11*, *26*), whereas ferric sulfide adducts of Bs-trHb and Tf-trHb are not reduced even by strong electron donors such as sodium dithionite. On the contrary, as reported previously, exposure of Bs-trHb to concentrated sodium dithionite solutions [> 10 mM (*10*)] results in the formation of a ferric hemoglobin sulfide adduct.

Sulfide binding to Bs-trHb and Tf-trHb has been demonstrated to occur in vivo within the *E. coli* host cells in which both proteins are recombinantly expressed (see Figure 1 and Figure S1 of the Supporting Information). Although no experimental evidence of the sulfide saturation state of trHbs within their original specimen is available to date, the high stability of the ferric sulfide adduct and the active sulfide metabolic turnover in bacteria suggest that an interaction between trHbs (when expressed) and the gaseous ligand is likely to occur in vivo and thus be physiologically relevant. As outlined in the introductory section, H$_2$S binding by trHbs certainly perturbs the equilibrium among the three main actors involved in the generation and scavenging of the gaseous ligand, namely, sulfite reductase, cysteine synthases, and the cysteine sensitive CysB gene regulator. The reported increase in the level of globin sulfide saturation under high oxygen growth conditions might be explained by the oxygen-dependent expression of cysteine synthase B (downregulated in the presence of oxygen). As the enzyme is a very effective sulfide scavenger under low oxygen conditions, it
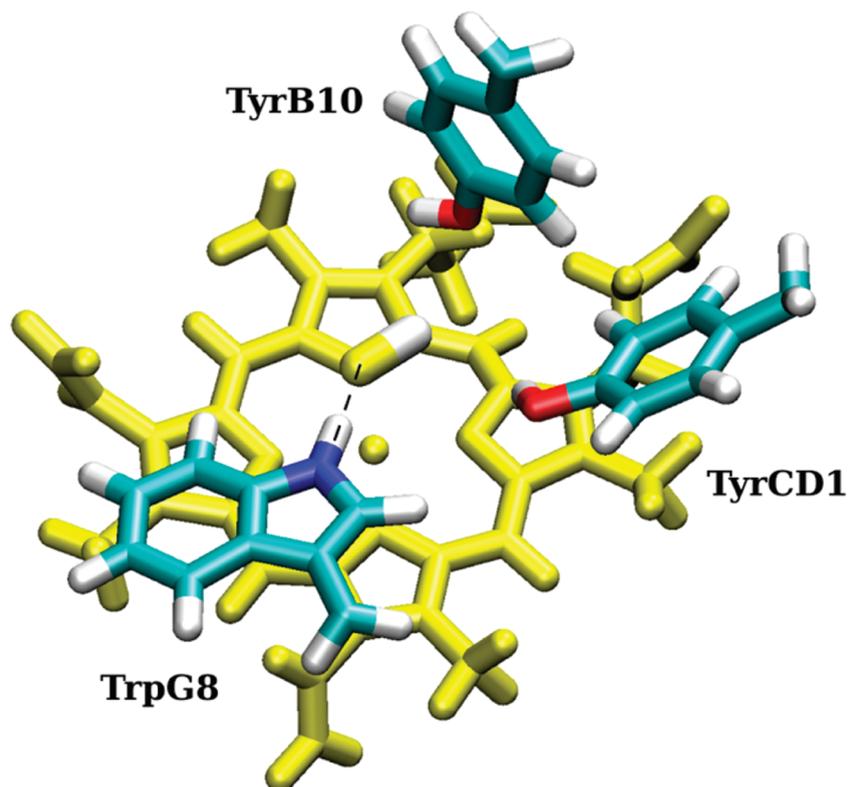
FIGURE 5: Schematic representation of the wt Tf-trHb distal site with coordinated SH⁻, showing the residues of the distal site (WG8, YCD1, and YB10).

might be hypothesized that it competes actively with expressed globins for the gaseous ligand, thus accounting for the lower level of sulfide saturation of recombinant hemoglobins during anaerobic growth. In contrast, the higher level of sulfide saturation of globins at high oxygenation levels might be attributed in part to the downregulation of the competing cysteine synthase B and in part to the highly oxidative environment that favors the oxidation of the trHbs, thus allowing prompt formation of the high-affinity ferric sulfide adduct. Nevertheless, the activity of sulfite oxidase must also be considered as it is the major source of H_2S within the bacterial cell. A dedicated study of the control of the expression of the enzyme in the presence of tr-Hbs will be necessary.

Besides a possible direct role of trHb in sulfide metabolism, an alternative hypothesis that suggests participation of these proteins in the control of the complex thiol redox pathway might be addressed. Interestingly, it has recently been demonstrated that the gene encoding Bs-trHb (as well as most trHbs from bacilli and staphylococci) is contained within a thiol redox pathway that is implicated in the bacterial response to the thiol oxidative stress (27). In particular, a postulated interaction has been proposed between Bs-trHb (*yjbI* gene) and a DsbA-like protein (similar to a disulfide bond redox catalyst, *yjbH* gene) whose gene is located upstream within the same operon in *B. subtilis*. Thus, Bs-trHb has been demonstrated to be co-expressed with the *yjbH* gene product and to be necessary for the control of global stress regulator Spx under disulfide stress (27). In this framework, one can envisage that Bs-trHb participates directly or indirectly in the complex redox pathway of sulfur metabolism in *Bacillus* sp. The mechanism of the Bs-trHb−YjbH interaction is currently under investigation.

The structural determinants for sulfide binding in bacterial trHbs can be traced back to the properties of the distal heme

cavity. The recently reported X-ray structures of Bs-trHb and Tf-trHb ferric derivatives (4, 5) revealed common structural features in the two proteins in that they are characterized by an array of aromatic residues surrounding the bound ligand: YB10 (25 in Bs-trHb and 54 in Tf-trHb), FCD1 (38) and YCD1 (67) in Bs-trHb and Tf-trHb, respectively, and WG8 (89 in Bs-trHb and 119 in Tf-trHb) (see Figure 7). The array of WG8, YB10, and YCD1 (in Tf-trHb) residues has been shown to be involved in a hydrogen bonding network with the iron-bound ligand and thus participate in the gaseous ligand stabilization. The architecture of the distal cavities of Bs-trHb and Tf-trHb can be compared with those of the few reported examples of sulfide binding heme proteins. The structure of the sulfide avid HbI from *L. pectinata* has shown that two phenyalanine residues occupy the positions corresponding to CD1 and E11 in myoglobin and the distal E7 residue is glutamine instead of the common histidine of vertebrate myoglobins and hemoglobins (28, 29). The structure of sulfide-bound HbI suggested two different kinds of interactions between the bound ligand and the relevant residues within the distal heme pocket, namely, H-bonding between sulfide and GlnE7 and sulfide−aromatic ring electrostatic interactions with PheCD1 and PheE11. These last interactions can be regarded as a major determinant of the high sulfide affinity of HbI on the basis of the reported weakness of H-bonds involving S atoms (30). On the other hand, Fe-bound sulfur has been described as a relatively strong H-bond acceptor in DFT calculations on thiolate-bound model porphyrins (31). Structural and functional comparisons of HbI with the homologous *L. pectinata* globins HbII and HbIII reveal that these last proteins do not share a high sulfide affinity with HbI and are thus regarded as regular oxygen carrier proteins (32). The origin of the ligand discrimination in the three proteins is as yet unknown, although the presence of TyrB10 in HbII and HbIII (PheB10 in HbI) has been proposed
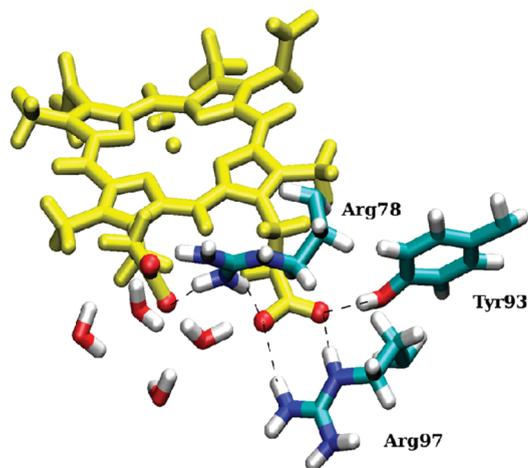
FIGURE 6: Schematic representation of the wt Tf-trHb distal site with coordinated SH⁻, showing the residues involved in the stabilization of heme propionates. Several water molecules interacting with the 7-propionyl are shown.
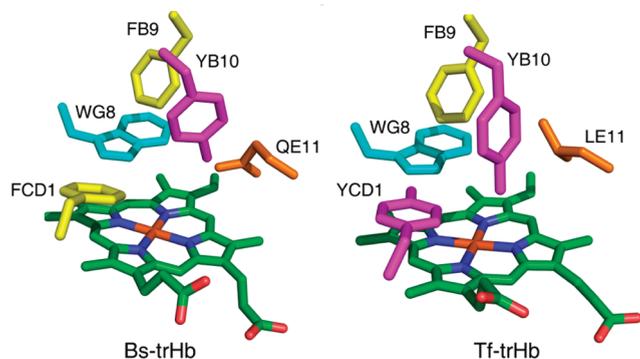

FIGURE 7: Close-up view of the distal pocket of Bs-trHb and Tf-trHb. The picture highlights the relevant FB9, YB10, and WG8 residues (common residues in both Bs-trHb and Tf-trHb) together with the protein specific residues within the distal heme pocket CD1 (Phe in Bs-trHb and Tyr in Tf-trHb) and E11 (Gln in Bs-trHb and Leu in Tf-trHb).

to destabilize sulfide binding (33) and stabilize preferentially oxygen through H-bonding. Consistently, a series of mutants of sperm whale myoglobin, which have been designed with the aim of obtaining model heme proteins with high affinity for sulfide, indicate that mutation of LeuB10 or ValE11 to Phe increases sulfide affinity 6-fold. Substitution of HisE7 with Gln, to generate the FQF triple mutant (His64Gln/Leu29Phe/Val68Phe), has been shown to be even more effective, such that the affinity of the FQF mutant for sulfide is 2 orders of magnitude higher than that of the native myoglobin (Table 2) (25). Direct hydrogen bonding between the GlnE7 carbonyl group and iron-bound sulfide has been postulated to be effective in determining the high sulfide affinity of the FQF Mb protein. It must be noted, though, that the effect of hydrogen bonding on the iron-bound sulfide is barely detectable in resonance Raman measurements of the Fe−S stretching frequencies in several heme protein sulfide adducts. Accordingly, we could not detect any relevant differences between the RR spectra of wild-type Tf-trHb and those of 3F-Tf-trHb and even *L. pectinata* Hb I (Figure 3 and Table 1), whereas it could be expected that the frequency of the ν(Fe−S) band shifts as an effect of interactions with the distal cavity residues. Moreover, while the WG8F single mutation affects the rate of sulfide release

(Tables 1 and 2), no significant differences are observed in the UV−vis and RR spectra of YCD1F and WG8F variants (Figure S3 of the Supporting Information) as compared to wt or the triple mutant. In particular, the frequency of the ν(Fe−S) stretching mode is not affected.

In summary, the presence of an aromatic cage and a hydrogen bond donor appear to account for the structural determinants that govern the thermodynamic properties of sulfide binding in hemoglobins. In this framework, the WG8, YB10, and Y/F CD1 triad in Tf-trHb and Bs-trHb provides the first shell of residues surrounding the coordinated sulfide but does not provide multiple H-bond interactions to the iron-bound ligand. In fact, kinetic data and molecular dynamics simulation indicate clearly that only WG8 residue contributes to the sulfide stabilization through H-bonding interaction, thus accounting for the relatively high affinity for sulfide in these proteins. In this manner, the effect of the triple mutation in 3F-Tf-trHb [10-fold increase in sulfide affinity (see Table 2)], which replaces putative hydrogen bonding interactions with a fully aromatic cage, strengthens the role of sulfide−aromatic interactions with respect to hydrogen bonding contributions and paves the way for the discussion of sulfide binding kinetics.

If the dissociation kinetics alone are considered (see Table 2), it appears that the replacement of the WG8, YB10, and Y/F CD1 triad with Phe residues in Tf-trHb makes the sulfide dissociation faster [by a factor of 100 (see Table 2)], which would imply a weakened stabilization of the iron-bound sulfide. This is in agreement with the idea that H-bonding is the main kinetic control of ligand dissociation in heme proteins and confirms the role exerted by WG8 on sulfide stabilization in truncated hemoglobins. In contrast, the very fast second-order rate of the sulfide combination reaction observed in 3F-trHb (∼20-fold faster than that measured for *L. pectinata* HbI) requires further comments. If we assume that the triple mutation does not alter significantly the overall architecture of the heme pocket, we may suggest that the aromatic cage provides an ideal environment for hydrogen sulfide to accommodate within the heme distal pocket while destabilizing iron-bound water. Distal pocket accessibility due to steric hindrance of the distal amino acids toward the bulky hydrogen sulfide molecule has been invoked to explain the slow sulfide binding rates in vertebrate hemoglobins (25, 26). Consistently, the flexibility of the GlnE7 distal residue was considered as a key factor in determining a relatively fast second-order combination rate in *L. pectinata* HbI (6). In 3F-trHb, however, the distal environment is certainly crowded and possibly rigid. Still the sulfide combination is even faster. Hence, there must be other relevant factors that modulate hydrogen sulfide entrance in the distal pocket. Molecular dynamics studies of the binding of sulfide to *L. pectinata* HbI and the FQF Mb mutant highlighted major favorable contributions to H_2S accommodation due to the unusual mobility of the heme macrocycle within the heme pocket in HbI, a dynamic behavior that is also partially reproduced in the FQF Mb mutant (32, 33). It is interesting to note that this dynamic model entails a high mobility of the propionate carbonyls that are suggested to be loosely hydrogen bonded to the polypeptide chain (67.66% occupancy) and rearrange considerably (weaken) upon sulfide binding (29.20% occupancy). In the case presented here, the resonance Raman spectra of Bs-trHb and Tf-trHB showed an upshift of the band at 383−384 cm⁻¹, assigned to heme propionyl bending vibrations, as a consequence of sulfide coordination. As mentioned in the Results, a shift to a higher frequency indicates a strengthened hydrogen bonding

between the propionyl groups of the heme and nearby amino acid side chains. Therefore, it can be inferred that a substantial rearrangement of the heme propionate geometry also occurs in Bs-trHb or Tf-trHb, upon sulfide binding. It is noteworthy that even when the simulation was performed in Tf-trHb but not in Bs-trHb, TrpG8 is located at the same position in both proteins, and moreover in Bs-trHb, TrpG8 is involved in the stabilization of CO and O_2 (*34*). That means that most likely, the relevance of TrpG8 to the stabilization of SH^- in Bs-trHb will be the same as in the case of Tf-trHb.

CONCLUSIONS

The key finding of this investigation concerns the ability of two group II truncated hemoglobins to bind sulfide with a relatively high affinity, such that they are partially saturated with sulfide when recombinantly expressed in *E. coli*. This observation paves the way for further investigations aimed at establishing the possible physiological relevance of the interaction between sulfides and truncated globins by monitoring expression levels of metabolically correlated enzymes such as sulfide reductase, cysteine synthases, and the CysB regulator. Moreover, the thermodynamic, kinetic, and spectroscopic data thus reported indicate that efficient sulfide binding can be achieved also within a distal pocket environment which bears little similarity to that typical of *L. pectinata* HbI. In particular, comparison of the sulfide binding properties between wt tf-trHb with the potential hydrogen bonding triad of YCD1, YB10, and WG8 and its triple Phe mutant provides the opportunity to dissect hydrogen bonding contributions from polar interactions to the iron-bound sulfide, thus offering a suitable model system for further structural and dynamics studies.

SUPPORTING INFORMATION AVAILABLE

Supplementary results, including the whole set of kinetic and thermodynamic experiments whose results are summarized in Table 2, UV−vis and resonance Raman spectra of single point mutants, protein spectra at different stages of purification, and background of molecular dynamics simulations. This material is available free of charge via the Internet at http://pubs.acs.org.

REFERENCES

1. Wittenberg, J. B., Bolognesi, M., Wittenberg, B. A., and Guertin, M. (2002) Truncated hemoglobins: A new family of hemoglobins widely distributed in bacteria, unicellular eukaryotes, and plants. *J. Biol. Chem.* 227, 871–874.
2. Wu, G., Wainwright, L. M., and Poole, R. K. (2003) Microbial globins. *Adv. Microb. Physiol.* 47, 255–310.
3. Giangiacomo, A., Ilari, L., Boffi, A., Morea, V., and Chiancone, E. (2005) The truncated oxygen-avid hemoglobin from *Bacillus subtilis*: X-ray structure and ligand binding properties. *J. Biol. Chem. 280*, 9192–9202.
4. Bonamore, A., Ilari, A., Giangiacomo, L., Bellelli, A., Morea, V., and Boffi, A. (2005) A novel thermostable hemoglobin from the actinobacterium *Thermobifida fusca*. *FEBS J. 272*, 4189–4201.
5. Ilari, A., Kjelgaard, P., von Wachenfeldt, C., Catacchio, B., Chiancone, E., and Boffi, A. (2007) Crystal structure and ligand binding properties of the truncated hemoglobin from *Geobacillus stearothermophilus*. *Arch. Biochem. Biophys. 457*, 85–94.
6. Milani, M., Pesce, A., Nardini, M., Ouellet, H., Ouellet, Y., Dewilde, S., Bocedi, A., Ascenzi, P., Guertin, M., Moens, L., Friedman, J. M., Wittenberg, J. B., and Bolognesi, M. (2005) Structural bases for heme binding and diatomic ligand recognition in truncated hemoglobins. *J. Inorg. Biochem. 99*, 97–109.
7. Milani, M., Savard, P. Y., Ouellet, H., Ascenzi, P., Guertin, M., and Bolognesi, M. (2003) A TyrCD1/TrpG8 hydrogen bond network and a TyrB10TyrCD1 covalent link shape the heme distal site of *Mycobacterium tuberculosis* hemoglobin O. *Proc. Natl. Acad. Sci. U.S.A. 100*, 5766–5771.
8. Ouellet, H., Juszczak, L., Dantsker, D., Samuni, U., Ouellet, Y. H., Savard, P.-Y., Wittenberg, J. B., Wittenberg, B. A., Friedman, J. M., and Guertin, M. (2003) Reactions of *Mycobacterium tuberculosis* truncated hemoglobin O with ligands reveal a novel ligand-inclusive hydrogen bond network. *Biochemistry 42*, 5764–5774.
9. Mukai, M., Savard, P. Y., Ouellet, H., Guertin, M., and Yeh, S. R. (2002) Unique ligand-protein interactions in a new truncated hemoglobin from *Mycobacterium tuberculosis*. *Biochemistry 41*, 3897–3905.
10. Feis, A., Lapini, A., Catacchio, B., Brogioni, S., Foggi, P., Chiancone, E., Boffi, A., and Smulevich, G. (2008) Unusually strong H-bonding to the heme ligand and fast geminate recombination dynamics of the carbon monoxide complex of *Bacillus subtilis* truncated hemoglobin. *Biochemistry 47*, 902–910.
11. Kraus, D. W., and Wittenberg, J. B. (1990) Hemoglobins of the *Lucina pectinata*/bacteria symbiosis. I. Molecular properties, kinetics and equilibria of reactions with ligands. *J. Biol. Chem. 265*, 6043–6053.
12. Boffi, A., Wittenberg, J. B., and Chiancone, E. (1997) Circular dichroism spectroscopy of Lucina I hemoglobin. *FEBS Lett. 411*, 335–338.
13. Siegel, L. M., and Davis, P. S. (1974) Reduced nicotinamide adenine dinucleotide phosphate-sulfite reductase of enterobacteria. IV. The *Escherichia coli* hemoflavoprotein: Subunit structure and dissociation into hemoprotein and flavoprotein components. *J. Biol. Chem. 249*, 1587–1598.
14. Nakamura, T., Iwahashi, H., and Eguchi, Y. (1984) Enzymatic proof for the identity of the S-sulfocysteine synthase and cysteine synthase B of *Salmonella typhimurium*. *J. Bacteriol. 158*, 1122–1127.
15. Filutowicz, M., Wiater, A., and Hulanicka, D. (1982) Delayed inducibility of sulphite reductase in cysM mutants of *Salmonella typhimurium* under anaerobic conditions. *J. Gen. Microbiol. 128*, 1791–1794.
16. Boyer, P. D. (1954) Spectrophotometric Study of the Reaction of Protein Sulfhydryl Groups with Organic Mercurials. *J. Am. Chem. Soc. 76*, 4331–4337.
17. Jorgensen, W. L., Chandrasekar, J., Madura, J., Impey, R. W., and Klein, M. L. (1983) Comparison of simple potential functions for simulating liquid water. *J. Chem. Phys. 79*, 926–935.
18. Luty, B. A., Tironi, I. G., and Van Gunsteren, W. F. (1995) Lattice-sum methods for calculating electrostatic interactions in molecular simulations. *J. Chem. Phys. 103*, 3014–3021.
19. Pearlman, D. A., Case, D. A., Caldwell, J. W., Ross, W. S., Cheatham, T. E., Debolt, S., Ferguson, D., Seibel, G., and Kollman, P. (1995) AMBER, a package of computer programs for applying molecular mechanics, normal mode analysis, molecular dynamics and free energy calculations to simulate the structural and energetic properties of molecules. *Comput. Phys. Commun. 91*, 1–41.
20. Crespo, A., Martí, M. A., Kalko, S. G., Morreale, A., Orozco, M., Gelpi, J. L., Luque, F. J., and Estrin, D. A. (2005) Theoretical study of the truncated hemoglobin HbN: Exploring the molecular basis of the NO detoxification mechanism. *J. Am. Chem. Soc. 127*, 4433–4444.
21. Cerda, J., Echevarria, Y., Morales, E., and Lopez-Garriga, J. (1999) Resonance Raman studies of the heme-ligand active site of haemoglobin I from *Lucina pectinata*. *Biospectroscopy 5*, 289–301.
22. Hu, S., Morris, I. K., Singh, J. P., Smith, K. M., and Spiro, T. G. (1993) Complete Assignment of Cytochrome c Resonance Raman Spectra via Enzymatic Reconstitution with Isotopically Labeled Hemes. *J. Am. Chem. Soc. 115*, 12466–12458.
23. Peterson, E. S., Friedman, J. M., Chienand, E. Y. T., and Sligar, S. G. (1998) Functional Implications of the Proximal Hydrogen-Bonding Network in Myoglobin: A Resonance Raman and Kinetic Study of Leu89, Ser92, His97, and F-Helix Swap Mutants. *Biochemistry 37*, 12301–12319.
24. Cerda-Colón, J. F., Silfa, E., and López-Garriga, J. (1998) Unusual Rocking Freedom of the Heme in the Hydrogen Sulfide-Binding Hemoglobin from *Lucina pectinata*. *J. Am. Chem. Soc. 120*, 9312–9317.
25. Nguyen, B. D., Zhao, X., Vyas, K., La Mar, G. N., Lile, R. A., Brucker, E. A., Phillips, G. N., Jr., Olson, J. S., and Wittenberg, J. B. (1998) Solution and crystal structures of a sperm whale myoglobin triple mutant that mimics the sulfide-binding hemoglobin from *Lucina pectinata*. *J. Biol. Chem. 273*, 9517–9526.
26. Pietri, R., Lewis, A., León, R. G., Casabona, G., Kiger, L., Yeh, S. R., Fernandez-Alberti, S., Marden, M. C., Cadilla, C. L., and López-Garriga, J. (2009) Factors Controlling the Reactivity of Hydrogen Sulfide with Hemoproteins. *Biochemistry 48*, 4881–4894.

27. Larsson, J. T., Rogstam, A., and von Wachenfeldt, C. (2007) YjbH is a novel negative effector of the disulfide stress regulator, Spx, in *Bacillus subtilis. Mol. Microbiol. 66*, 669–684.

28. Rizzi, M., Wittenberg, J. B., Coda, A., Fasano, M., Ascenzi, P., and Bolognesi, M. (1994) Structure of the sulfide-reactive hemoglobin from the clam *Lucina pectinata*: Crystallographic analysis at 1.5 Å resolution. *J. Mol. Biol. 244*, 86–99.

29. Rizzi, M., Wittenberg, J. B., Coda, A., Ascenzi, P., and Bolognesi, M. (1996) Structural bases for sulfide recognition in *Lucina pectinata* hemoglobin I. *J. Mol. Biol. 258*, 1–5.

30. Biswal, H. S., Shirhatti, P. R., and Wategaonkar, S. (2009) O-H···O versus O-H···S Hydrogen Bonding I: Experimental and Computational Studies on the p-Cresol·H_2O and p-Cresol·H_2S Complexes. *J. Phys. Chem. A 113*, 5633–5664.

31. Dey, A., Okamura, T.-a., Ueyama, N., Hedman, B., Hodgson, K. O., and Solomon, E. I. (2005) Sulfur K-edge XAS and DFT calculations on P450 model complexes: Effects of hydrogen bonding on electronic structure and redox potentials. *J. Am. Chem. Soc. 127*, 12046–12053.

32. Gavira, J. A., Camara-Artigas, A., De Jesus-Bonilla, W., Lopez-Garriga, J., Lewis, A., Pietri, R., Yeh, S.-R., Cadilla, C. L., and Garcýa-Ruiz, J. M. (2008) Structure and ligand selection of hemoglobin II from *Lucina pectinata*. *J. Biol. Chem. 283*, 9414–9423.

33. Fernandez-Alberti, S., Bacelo, D. E., Binning, R. C., Jr., Echave, J., Chergui, M., and Lopez-Garriga, J. (2006) Sulfide-binding hemoglobins: Effects of mutations on active-site flexibility. *Biophys. J. 91*, 1698–1709.

34. Boechi, L., Mañez, P. A., Luque, F. J., Marti, M. A., and Estrin, D. A. (2010) Unraveling the molecular basis for ligand binding in truncated hemoglobins: The trHbO *Bacillus subtilis* case. *Proteins 78*, 962–970.

35. Champion, P. M., Stallard, B. R., Wagner, G. C., and Gunsalus, I. C. (1982) Resonance Raman Detection of an Fe-S Bond in Cytochrome P450cam. *J. Am. Chem. Soc. 104*, 5469–5472.

36. Bangcharoenpaurpong, O., Hall, K. S., Hager, L. P., and Champion, P. M. (1986) Resonance Raman studies of isotopically labeled chloroperoxidase. *Biochemistry 25*, 2374–2378.

37. Santolini, J., Roman, M., Stuehr, D. J., and Mattioli, T. A. (2006) Resonance Raman study of *Bacillus subtilis* NO synthase-like protein: Similarities and differences with mammalian NO synthases. *Biochemistry 45*, 1480–1489.

38. Schelvis, J. P., Berka, V., Babcock, G. T., and Tsai, A. L. (2002) Resonance Raman detection of the Fe-S bond in endothelial nitric oxide synthase. *Biochemistry 41*, 5695–5701.

39. Todorovic, S., Rodrigues, J. V., Pinto, A. F., Thomsen, C., Hildebrandt, P., Teixeira, M., and Murgida, D. H. (2009) Resonance Raman study of the superoxide reductase from *Archaeoglobus fulgidus*, E12 mutants and a 'natural variant'. *Phys. Chem. Chem. Phys. 11*, 1809–1815.

40. Leu, B. M., Ching, T. H., Zhao, J., Sturhahn, W., Alp, E. E., and Sage, J. T. (2009) Vibrational Dynamics of Iron in Cytochrome c. *J. Phys. Chem. B 113*, 2193–2200.